# The relationship between kurtosis- and envelope-based indexes for the diagnostic of rolling element bearings

P. Borghesani *, P. Pennacchi, S. Chatterton

*Politecnico di Milano, Dipartimento di Meccanica, Via la Masa 1, 20156 Milano, Italy*

Received 19 June 2013
Received in revised form
24 September 2013
Accepted 6 October 2013
Available online 5 November 2013

## 1. Introduction

In many machine components, when damage occurs, a strongly impulsive signal is generated, triggering a series of vibrations according to the impulse response function of the structure of the mechanical system where the component is installed. This behavior is, for instance, typical of internal combustion engines [1], rolling element bearings [2], fluid instability phenomena in hydraulic and steam turbines [3–6] and rubbing phenomena in large turbomachineries [7,8].

*Abbreviations:* AS, autospectrum; BPFI, ball pass frequency inner; BPFO, ball pass frequency outer; CS2, second order cyclostationary; CPW, cepstrum pre-whitening; DFT, discrete Fourier transform; FFT, fast Fourier transform; IDFT, inverse discrete Fourier transform; IEPE, integrated electronics piezo-electric; IFFT, inverse fast Fourier transform; IIR, infinite impulse response; NSES, normalized squared envelope spectrum; RCC, ratio of cyclic content; RMS, root mean square; SE, squared envelope; SES, squared envelope spectrum

* Corresponding author. Tel.: +39 2 2399 8486.
*E-mail address:* pietro.borghesani@mail.polimi.it (P. Borghesani).

In the last years, two main families of signal processing tools have gained a leading role in the diagnostic of such components: the kurtosis-based family and the CS2 family.

The first family consists of time and frequency domain indexes derived from the kurtosis index, which is chosen as a direct measure of the “impulsiveness” of the signal [10]. Kurtosis, band kurtosis, spectral kurtosis and kurtogram are the most used techniques belonging to this category. The spectral kurtosis, presented by Dwyer [11], has been indicated as a very effective tool for the identification of transients in a signal, representing, in the case of diagnostics, the response of the system to impulsive excitation due to the damage; however, the complexity of its calculation hindered its diffusion in industrial application. On the contrary, the kurtogram, introduced in this field by Antoni and Randall [12], has been further developed to ease its calculation in the so called Fast Kurtogram [13] and consequently represents an efficient tool to select the best band for the filtering step in the process of envelope analysis. Improved results have been shown for a higher-resolution kurtosis-based index, the protrugram, developed by Barszcz and Jabłoński [14]. This index is obtained by calculating the kurtosis of the analytic signal on a narrow band, which is shifted almost continuously along the frequency axis.

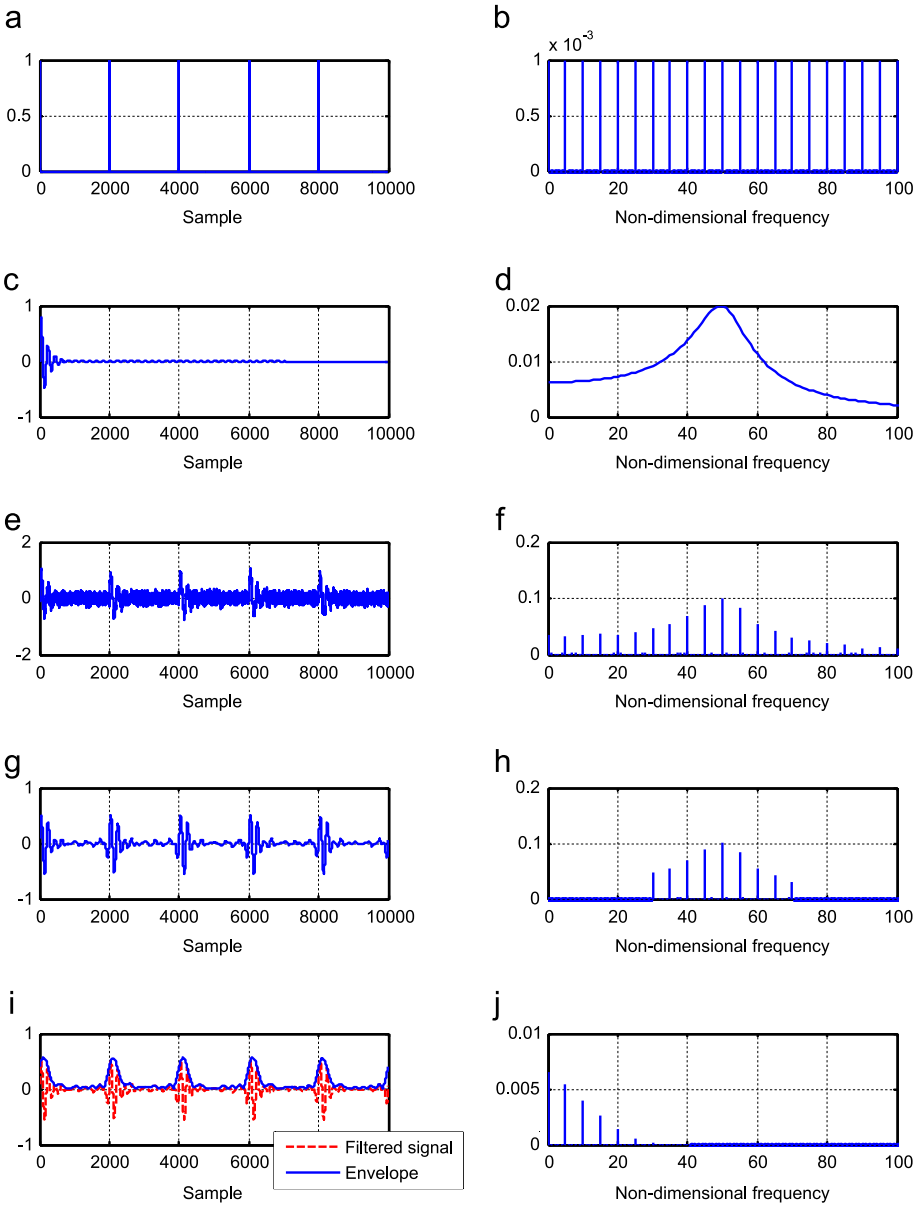


**Fig. 1.** Simulated signal of in case of an impulsive excitation on a 1 d.o.f. mechanical system: (a) impulse train in time domain, (b) impulse train in frequency domain, (c) impulse response of the system in time domain, (d) impulse response of the system in frequency domain, (e) simulated signal as convolution of impulse train and impulse response with additional white noise, (f) simulated signal in frequency domain, (g) filtered simulated signal in time domain, (h) filtered simulated signal in frequency domain, (i) envelope in time domain, and (j) SES.

The second family of diagnostic tools is represented by the cyclostationary group, among which the envelope and the squared envelope spectrum (SES) are the most widely spread in the industrial applications for the diagnostics of impulsive signals, i.e. CS2. Such techniques have been thoroughly described and analyzed in the field of rotating machineries, and especially in bearing diagnostics [15,16]. The basic idea of this approach is to treat the signal as a stochastic quantity, whose variance (i.e. energy, squared value) varies cyclically as a function of time or of the angular rotation of a reference shaft. In fact, when the impulsive excitation triggers the natural vibration of the mechanical structure, the energy in the signal is expected to increase with respect to the average energy level associated to normal conditions. The procedure to obtain the SES consists of 3 steps [17]:

1. The signal is filtered around a resonance in order to remove noise and highlight the natural vibrations of the structure, which has been caused by the impulsive excitation of the damage.
2. The squared-envelope (SE) signal is calculated as squared absolute value of the analytic signal, obtained by means of the Hilbert transform applied to the filtered signal. This operation is expressed in Eq. (1), where $x_f$ is the band-pass filtered signal and $j$ is the imaginary unit

$$\mathrm{SE}_x[n] = |x_f[n] + j \cdot \mathrm{Hilbert}\{x_f[n]\}|^2 \tag{1}$$

3. The SES is finally obtained as the autospectrum of the square of the envelope signal, i.e. as the squared absolute value of the discrete Fourier transform (DFT) of the envelope:

$$\mathrm{SES}_x[k] = |\mathrm{DFT}\{\mathrm{SE}_x[n]\}|^2 \tag{2}$$

For the sake of clarity, an example of damage symptomatic signal has been numerically simulated and analyzed by means of the envelope in Fig. 1.

- An impulse train has been generated with a constant period: time domain (a) and frequency domain (b).
- It has been convolved with an impulse response function: time domain (c) and frequency domain (d).
- White noise has been added to the result of the convolution, representing the simulated measurement: time domain (e) and frequency domain (f).
- The signal has been band-pass filtered around the resonance (30–70 non-dimensional frequency): time domain (g) and frequency domain (h).
- The absolute value of the analytic signal has been calculated by means of the Hilbert transform, obtaining the envelope signal (i) and the corresponding squared envelope spectrum (SES) (j).

In the past, the two families have often been coupled, in multi-steps signal processing procedures. A typical combination is the selection of the pass-band filter by means of the kurtogram [13] or protrugram [14], identifying the "most impulsive" (i.e. highest kurtosis) band for the application of the envelope analysis. This approach was found successful by many authors in different experimental applications in the past (e.g. [18–20]). However, the two families have always been treated on the basis of two different analytical bases, one referring to the "impulsiveness" of the signal, the other to the cyclic 2nd order statistics of the signal.

Moreover, while envelope analysis has been indicated as the main tool for a detailed diagnostic of faults, simple kurtosis-based indexes have usually been implemented in prognostics, being naturally easier to track on a long time span.

The aim of this paper is to demonstrate the analytical connection among kurtosis and SES, giving a single analytical framework for the analysis of diagnostic of impulsive machine signals, and to identify the most suitable indicators for diagnostic and prognostics. The paper will analyze the properties of general signals such as that of Fig. 1, to obtain the analytical equivalencies among kurtosis and envelope indexes. Thus, an experimental campaign on rolling element bearings will be presented to finally identify the analogies and differences of kurtosis and envelope based prognostic strategies.

## 2. Analytical identities

### 2.1. Kurtosis and envelope

As mentioned in the previous section, the first step of envelope analysis results in a band-pass filtered vibration signal $x_f[n]$, consisting of a convolution of the measured signal $x[n]$ with the filter $f_l^h[n]$, which is selected as an ideal pass-band filter with non-dimensional pass-band $l \le k < h$

$$x_{l,h}[n] = x[n] \otimes f_l^h[n] \tag{3}$$

Then the analytic signal $\tilde{x}[n]$ is obtained as follows:

$$\tilde{x}_{l,h}[n] = x_{l,h}[n] + j \cdot \mathrm{Hilbert}\{x_{l,h}[n]\} \tag{4}$$

Such signal will have the following DFT:

$$\mathrm{DFT}\{\tilde{x}_{l,h}[k]\} = \begin{cases} 2\mathrm{DFT}\{x_{l,h}[k]\} & l \le k < h \\ 0 & \text{otherwise} \end{cases} \tag{5}$$

The sample kurtosis $\kappa_{l,h}$ of this signal is defined as the ratio among the fourth central moment $m_4$ and the squared second central moment $m_2$ of $\tilde{x}_{l,h}[n]$:

$$\kappa_{l,h} = \frac{m_4\{\tilde{x}_{l,h}[n]\}}{(m_2\{\tilde{x}_{l,h}[n]\})^2} \tag{6}$$

Since vibration signals are generally expected to be zero-mean, the numerator, or fourth moment, is estimated by the following:

$$m_4\{\tilde{x}_{l,h}[n]\} = \frac{1}{N}\sum_{n=1}^{N} |\tilde{x}_{l,h}[n]|^4 \tag{7}$$

The right hand side of Eq. (7) can be rewritten in the following form:

$$m_4\{\tilde{x}_{l,h}[n]\} = \frac{1}{N}\sum_{n=1}^{N} (|\tilde{x}_{l,h}[n]|^2)^2 \tag{8}$$

In this form, it is possible to identify the SE signal (see Eq.. (1)), which can be substituted in the equation, giving:

$$m_4\{\tilde{x}_{l,h}[n]\} = \frac{1}{N}\sum_{n=1}^{N} (\mathrm{SE}_{l,h}[n])^2 \tag{9}$$

And, by applying Parseval's theorem [21], it results in the following equation:

$$m_4\{\tilde{x}_{l,h}[n]\} = \sum_{n=1}^{N} |\mathrm{DFT}\{\mathrm{SE}_{l,h}[n]\}|^2 \tag{10}$$

The right hand term of (10) exactly matches the definition of the SES (see Eq. (2)), thus, by considering that SES (in its single-sided form) is non-zero only in the range of cyclic frequencies $0 \le k < h-l$ it is possible to state a first significant identity:

$$\sum_{k=0}^{h-l} \mathrm{SES}_{l,h}[k] = m_4\{\tilde{x}[n]\} \tag{11}$$

Therefore, Eq. (6) can be rewritten, by considering Eq. (11) and by expressing the denominator as the fourth power of the root mean square (RMS) of the filtered analytic signal (see Appendix A for proof):

$$\kappa_{l,h} = \frac{\sum_{k=0}^{h-l}\mathrm{SES}_{l,h}[k]}{\mathrm{RMS}_{l,h}^4} \tag{12}$$

By similar (even easier) steps it is possible to demonstrate that the denominator of Eq. (6) is equivalent to the sum of squares of the autospectrum of the analytic signal, in turn equal to the zero frequency value of the SES. Thus, an alternative form of Eq. (12) is as follows:

$$\kappa_{\tilde{x}} = \frac{\sum_{k=0}^{h-l}\mathrm{SES}_{l,h}[k]}{\left(\sum_{k=l}^{h}|\mathrm{AS}_{l,h}[k]|^2\right)^2} = \frac{\sum_{k=0}^{l-h}\mathrm{SES}_{l,h}[k]}{\mathrm{SES}_{l,h}[0]} \tag{13}$$

The definition of the Fast Kurtogram exactly matches that of the kurtosis of the analytic signal of the pass-band filtered vibration (Eq. (6)) and has been often used as an index of impulsiveness of the signal in such band. In different papers [14], a very similar quantity is used, from which Eq. (13) only differs because the analytic signal is considered instead of the original band-pass filtered vibration signal. This has usually little relevance and, even if an analytical equivalence is difficult to be obtained, the results are often similar and just scaled with a factor of 1.5.

Moreover, the denominator of Eq. (13) is recognizable in the scale factor which Antoni proposes in order to assess the SES and identify CS2 peaks. In light of this consideration, Eq. (12) now explains with a stronger analytical basis why the band-kurtosis and the kurtogram have proven so effective in selecting the best band for the envelope analysis. In fact, the kurtosis of a single band, selected for the calculation of the envelope, will be high if the peaks of the corresponding SES (i.e. numerator of Eq. (12)) are significantly above the SES average expected value (proportional to the numerator of Eq. (12)).

### 2.2. Cepstrum pre-whitening

The recognition of the SES in Eq. (12), normalized with the threshold proposed by Antoni in [15], leads to a further interesting consideration. In fact, by considering the normalized SES, it is possible to write:

$$\mathrm{NSES}_{l,h}[k] = \frac{|\mathrm{DFT}\{|\tilde{x}_{l,h}[n]|^2\}|^2}{\mathrm{RMS}_{l,h}^4} \tag{14}$$

and, by including the denominator in the numerator:

$$\mathrm{NSES}_{l,h}[k] = \left|\mathrm{DFT}\left\{\frac{|\tilde{x}_{l,h}[n]|^2}{\mathrm{RMS}_{l,h}^2}\right\}\right|^2 \tag{15}$$

If the band-pass filtering is taken to the limit of a single spectral line, the RMS of the so-obtained mono-harmonic signal coincides with the amplitude of the harmonics itself, thus, the scalar-valued NSES (only the zero frequency is non-zero) is expressed by the following:

$$\mathrm{NSES}_{l,l+1} = \left|\mathrm{DFT}\left\{\left(\frac{|\tilde{x}_{l,l+1}[n]|}{|\tilde{X}[l]|}\right)^2\right\}\right|^2, \quad \tilde{X}[k] = \mathrm{DFT}\{\tilde{x}[n]\} \tag{16}$$

By rearranging the fraction in the parentheses, the following equation is obtained:

$$\mathrm{NSES}_{l,l+1} = \left|\mathrm{DFT}\left\{\left|\mathrm{IDFT}\ \frac{\tilde{X}[l]}{|\tilde{X}[l]|}\right)\right|^2\right\}\right|^2 \tag{17}$$

Cepstrum pre-whitening was in the first place introduced by Sawalhi and Randall [22], based on the real cepstrum:

$$C[n] = \mathrm{IDFT}\{\log|\mathrm{DFT}(x[n])|\} \tag{18}$$

Peaks in the absolute value of the real cepstrum indicate the presence of a deterministic multi-harmonic component in the signal. The pre-whitening operation consists in setting a zero value for the whole real cepstrum (except possibly at zero quefrency), then, once transformed back to the frequency domain, the obtained signal is recombined with the phase of the original signal and inverse transformed to time domain.

This procedure can also be implemented in a very simple way (see for instance [23,24]), avoiding the transformation to the cepstral domain, just by dividing the Fourier transformed signal by its absolute value and transforming back to the time domain.

$$x_{cpw}[n] = \mathrm{IDFT}\left\{\frac{\mathrm{DFT}(x[n])}{|\mathrm{DFT}(x[n])|}\right\} \tag{19}$$

Thus, recognizing in Eq. (17) the expression of the cepstrum pre-whitening (CPW), it is finally possible to express the following identity for the squared envelope spectrum of the CPW signal $\mathrm{SES}_{CPW}[k]$:

$$\mathrm{SES}_{\mathrm{CPW}}[k] = \mathrm{NSES}_{k,k+1} = \left|\mathrm{DFT}\left\{\left|\mathrm{IDFT}\ \frac{\tilde{X}[k]}{|\tilde{X}[k]|}\right)\right|^2\right\}\right|^2 \tag{20}$$

## 3. A new method for the selection of the optimal demodulation band

The analytical results of Section 2.1 suggest a possible improvement in the choice of the optimal demodulation band by means of kurtosis-based methods. As demonstrated above, the kurtogram, if calculated on the analytic signal, exactly matches the sum of all peaks of the SES. Thus, this tool is a very good solution only if the bearing fault is the only source of CS2 components.

Unfortunately, in complex industrial system, such as servomotors, traction systems, or pumping plants, CS2 sources may be different and sometimes prevailing over incipient bearing fault symptoms. Moreover, if the carriers of such "disturbances" are different from those of the bearing signal in terms of spectral support, the kurtogram may lead to a wrong selection of the band.

This problem may be strongly reduced by looking at the contribution to the kurtosis of a specific band, symptomatic of a bearing fault, rather than at the raw value of the kurtosis itself.

A cyclic band kurtosis may be defined, by extending the definition of the full kurtosis of Eq. (12) as follows:

$$\kappa_{l,h}^{p,q} = \frac{\sum_{k=p}^{q} \mathrm{SES}_{l,h}[k]}{\mathrm{RMS}_{l,h}^4} \tag{21}$$

where $l, h$ represent the spectral filtering of the signal, while the cyclic bands $p, q$ limit the integration of the SES. Therefore, this index represents the normalized sum of the SES peaks in the cyclic range $p, q$. If a narrow cyclic band is chosen around the characteristic frequency of a bearing damage, the result will be a good estimate the total amount of second order cyclostationarity associated to the bearing.

It is important to underline the substantial difference in the two domains of definition of $l, h$ and $p, q$: if the first range corresponds to a sets of discrete spectral frequencies, i.e. in the classical Fourier approach to signal analysis, the second range represents a set of cyclic frequencies, identifying periodicities not in the signal itself but in its second statistical moment, i.e. Fourier transform of the signal's power.

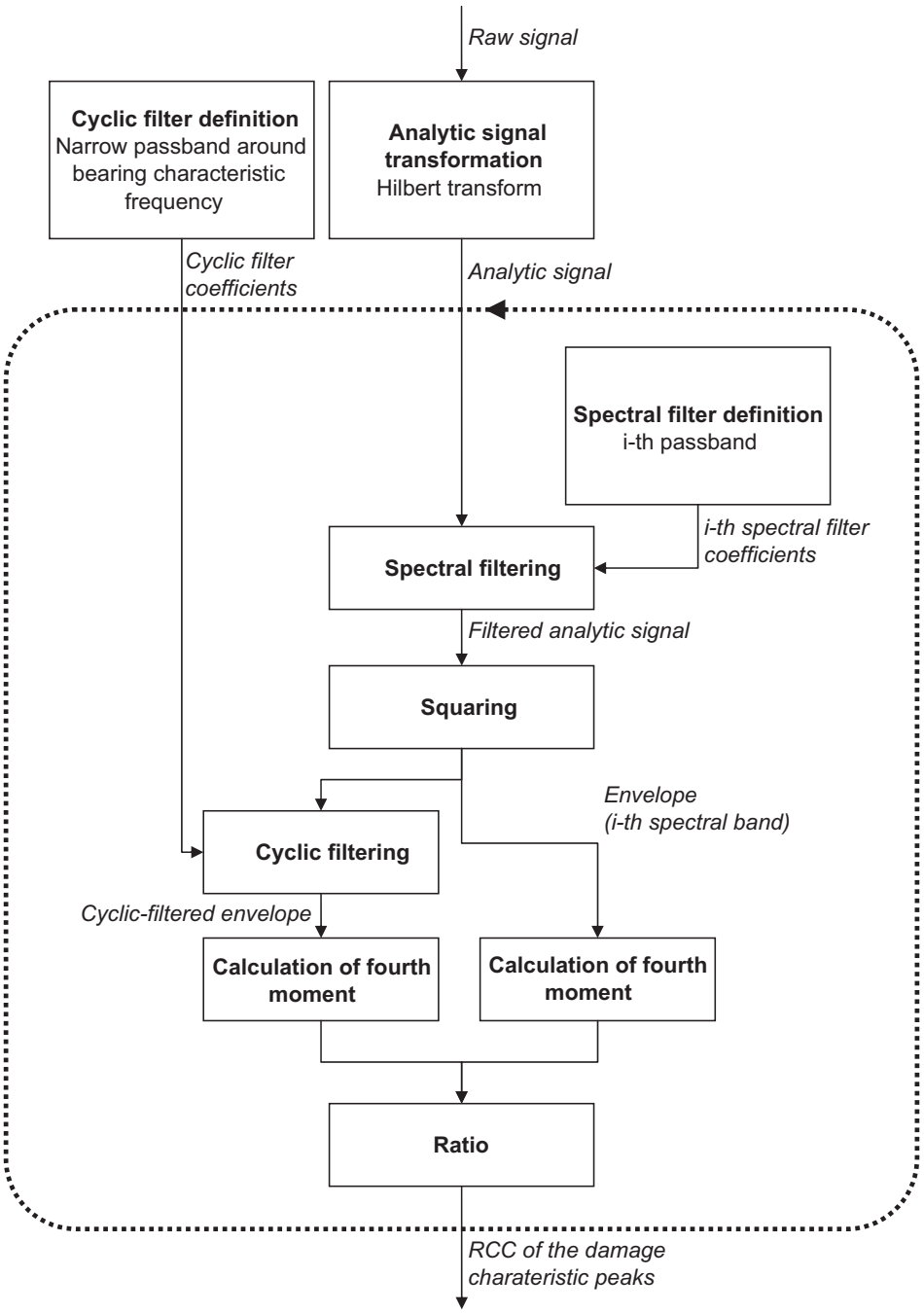


**Fig. 2.** Block diagram for the calculation of the RCC index.

Thus, the ratio of cyclic content (RCC) associated to the cyclic band $(p,q)$, with a spectral support on $(l,h)$ may be expressed as follows:

$$\mathrm{RCC}_{l,h}^{p,q} = \frac{\kappa_{l,h}^{p,q}}{\kappa_{l,h}} = \frac{\sum_{k=p}^{q} \mathrm{SES}_{l,h}[k]}{\sum_{k=0}^{h-l} \mathrm{SES}_{l,h}[k]} \tag{22}$$

where $(l,h)$ are the lower and upper bounds of the spectral filter applied to calculate the envelope signal, while $(p,q)$ delimitate the normalized cyclic frequency range for the integration of the kurtosis contribution.

The calculation of such index does not require the full computation of the SES, which would make it a trivial *a posteriori* tool. In fact the procedure may be simplified significantly considering that the kurtosis of the raw signal is in general very similar to the kurtosis of the corresponding analytic signal. Therefore, an estimate of RCC is obtained by applying fast

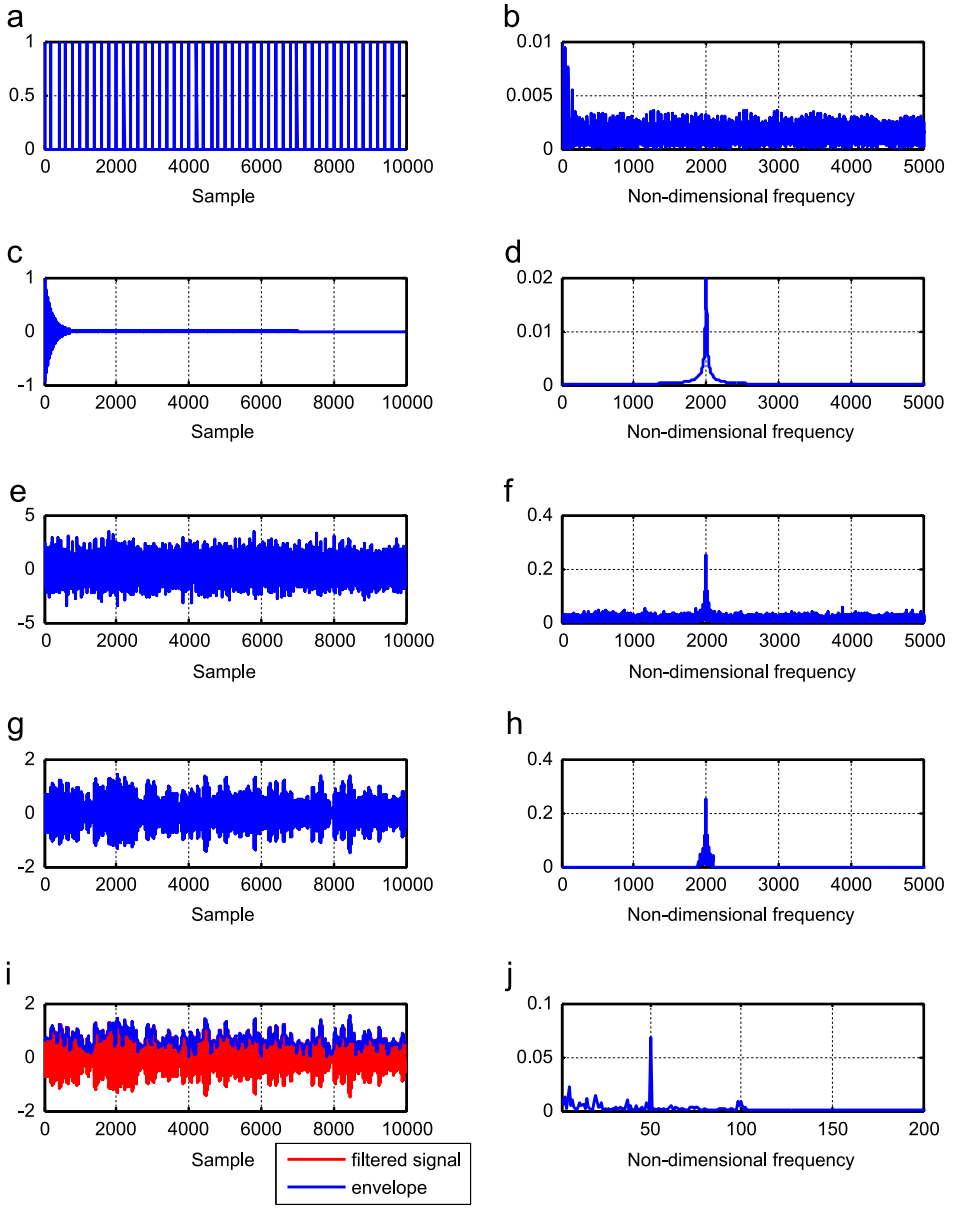


**Fig. 3.** Numerical simulation of a bearing signal: (a and b) impulse train with 5% (standard deviation) jitter in time and frequency domain, (c and d) 1 d.o.f. impulse response and frequency response function, (e and f) time and frequency domain signal obtained by convolution of (a) and (c) with additional noise, (g and h) time and frequency domain representation of the signal (e) after band-pass filtering in the range [1900 2100], and (i and j) envelope and squared envelope spectrum.

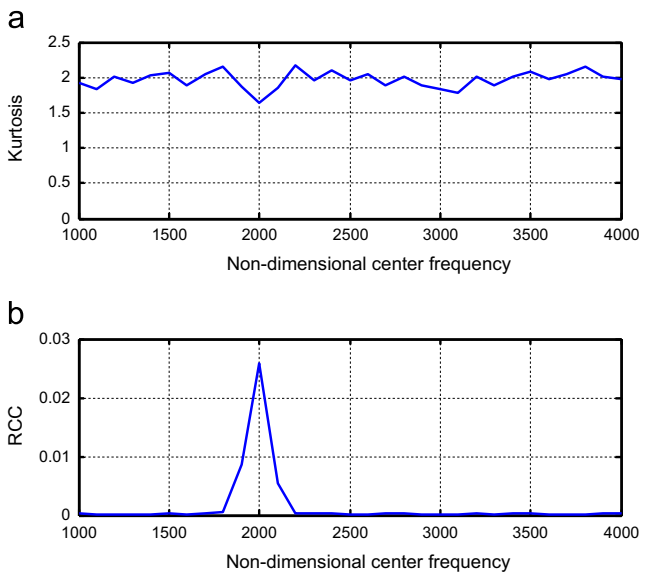


**Fig. 4.** Numerical simulation of a bearing signal: (a) band kurtosis and (b) band RCC in the cyclic range [40:60].

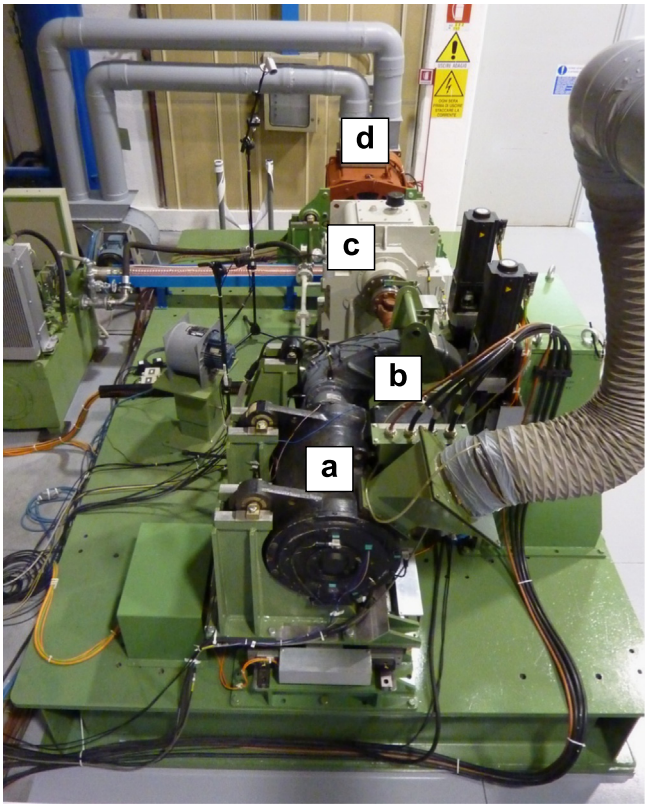


**Fig. 5.** Test-rig: (a) traction motor, (b) gearbox, (c) additional gearbox, and (d) breaking motor.

band-pass filters, designed for instance with Butterworth's approach:

$$\mathrm{RCC}_{l,h}^{p,q} \approx \frac{\frac{1}{N}\sum_{n=1}^{N}\{(|x[n] \otimes \mathrm{FILTER}(l,h)|^2) \otimes \mathrm{FILTER}(p,q)\}^2}{\frac{1}{N}\sum_{n=1}^{N}(|x[n] \otimes \mathrm{FILTER}(l,h)|^2)^2} \tag{23}$$

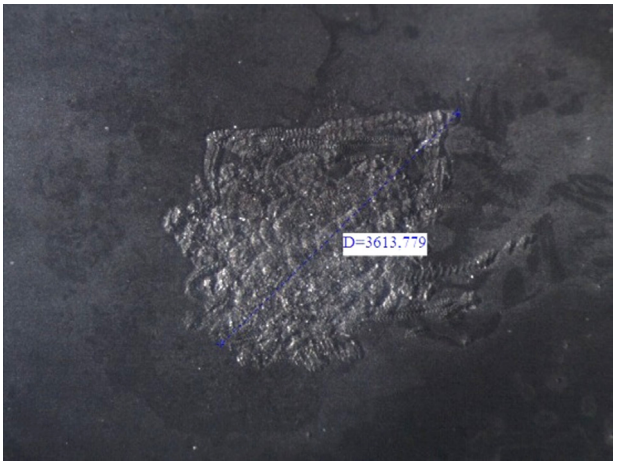


**Fig. 6.** Damage on the inner ring.

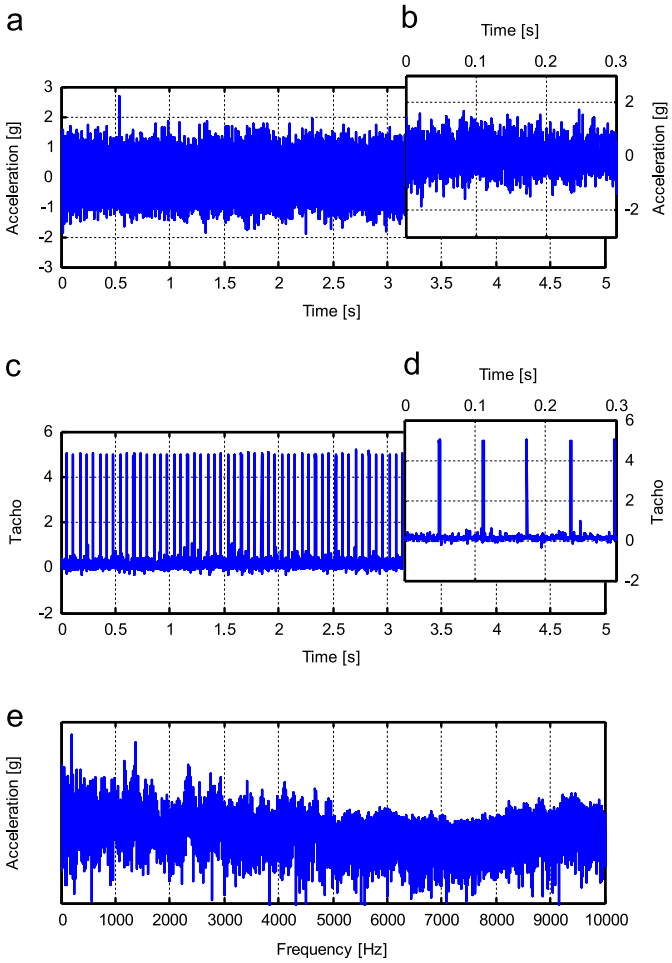


**Fig. 7.** First test – (a) raw accelerometer signal, (b) zoom of the raw accelerometer signal, (c) raw tachometer signal, (d) zoom of the raw tachometer signal, and (e) spectrum of the raw accelerometer signal.

Moreover, the spectral filter may be calculated only once and used for a series of $(l_i, h_i)$ spectral pass-bands, in order to obtain a kurtogram or protrugram. The procedure is detailed in Fig. 2.

Alternatively, if the cyclic pass-band is composed by few cyclic frequency lines, it is possible to exactly calculate the numerator of Eq. (22) by exploiting the relationship between the envelope spectrum and the spectral correlation [25].

In particular:

$$\mathrm{RCC}_{l,h}^{p,q} = \frac{16\sum_{n=p}^{q}\left|\sum_{k=l}^{h-k} X[k]X^{*}[k+n]\right|^{2}}{\frac{1}{N}\sum_{n=1}^{N}(|\tilde{x}_{l,h}[n]|^{2})^{2}}, \quad X[k] = \mathrm{DFT}\{x[n]\} \tag{24}$$

where the coefficient 16 is due to the fact that the DFT of the signal $x[n]$ is here used instead of the DFT of the analytic signal $\tilde{x}[n]$. The numerical efficiency of this procedure, working for all spectral bands on the same $X[k]$, has to be compared with the fully time-domain process presented in Fig. 2. The best choice depends strongly on the implementation of the two and on the width of the cyclic pass-band.

## 4. Numerical validation

A 10,000 point long numerical signal, simulating the real behavior of a rolling element bearing, was generated in order to provide a first validation of the analytical results produced in the previous sections. First of all, an impulse train was obtained with an average period of 200 points (non-dimensional frequency of 50) and a zero-mean, delta correlated jitter, whose standard deviation has been set to 5% of the period (see Fig. 3(a) and (b)). This impulse train has been convolved with the typical impulse response a 1 d.o.f. mechanical system, with natural non-dimensional frequency of 2000 and damping ratio of 0.5% (Fig. 3(c) and (d)). The so-obtained signal is represented in Fig. 3(e) and (f), after the addition of a background noise with zero- mean and 0.8 standard deviation. The correct pass-band for the calculation of the SES is in this case known, given the exact knowledge of this simple system, and has a central frequency that coincides with the natural frequency of the frequency response function (2000). A bandwidth of 201 spectral points has been chosen for the band-pass filter, representing a number sufficiently greater than the cyclic frequency of the phenomenon (50). The result of the filtering operation is shown in Fig. 3(g) and (h). Finally the envelope of Fig. 3(i) is calculated by the Hilbert transform and the SES of

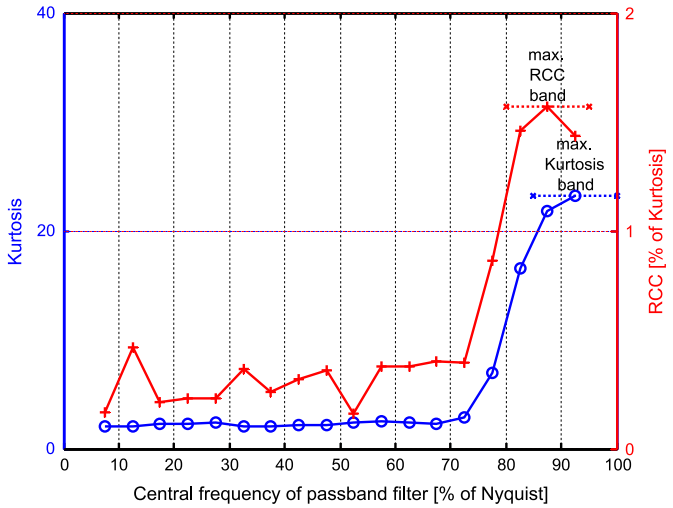


**Fig. 8.** First test – band selection for the calculation of the SES: comparison among kurtosis and RCC method (ideal digital filters have been used). (For interpretation of the references to color in this figure caption, the reader is referred to the web version of this paper.)

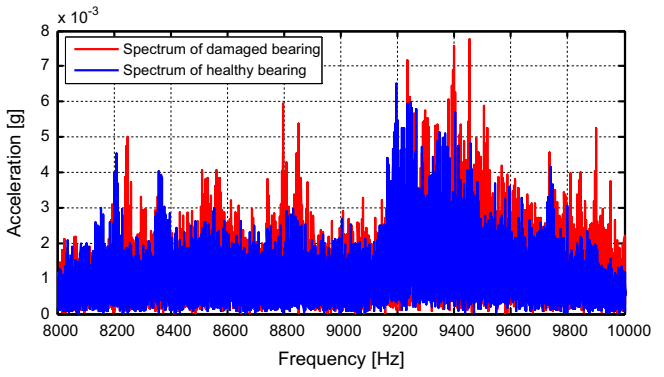


**Fig. 9.** First test – comparison of the spectra of healthy and damaged bearing.

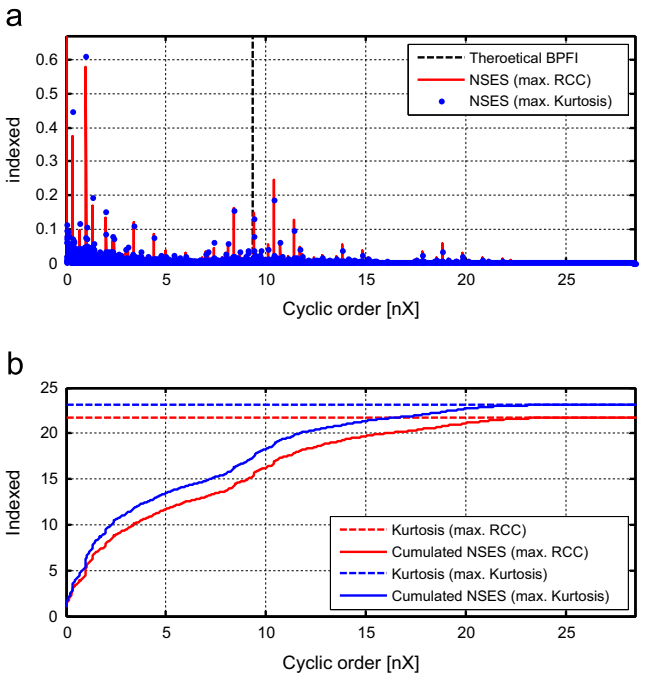


**Fig. 10.** First test – comparison among optimal kurtosis band and optimal RCC band: (a) normalized SES and (b) cumulated tests and kurtosis. (For interpretation of the references to color in this figure caption, the reader is referred to the web version of this paper.)

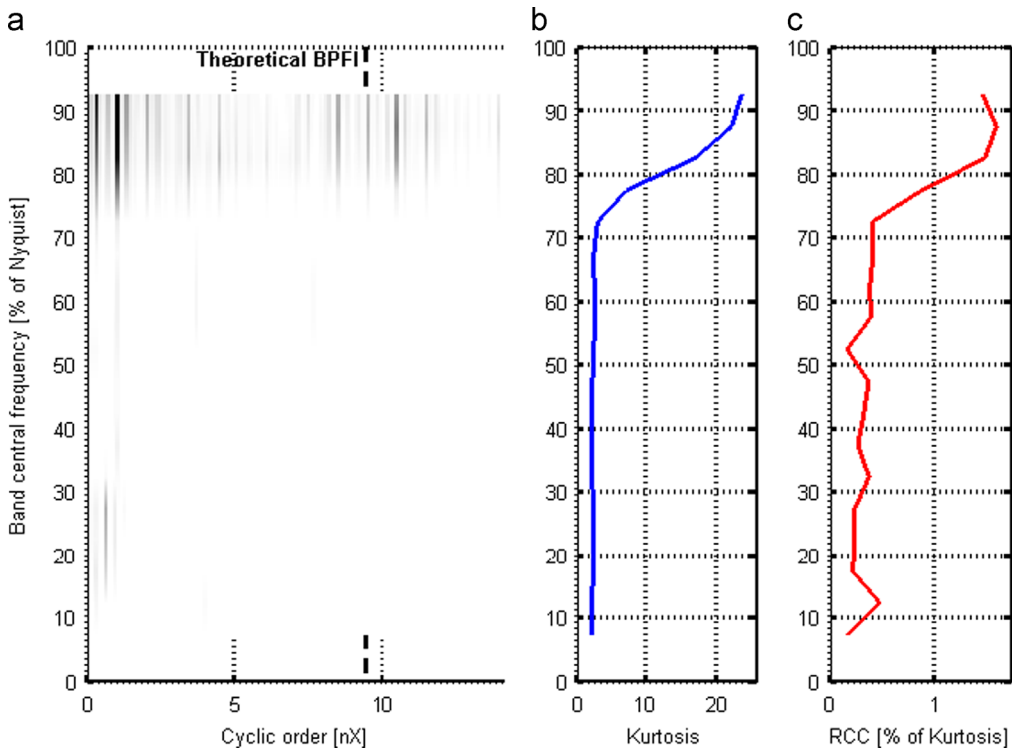


**Fig. 11.** First test – comparison: (a) normalized SES for different demodulation bands, (b) corresponding kurtosis of the band-pass filtered analytic signal, and (c) corresponding RCC of the cyclic band 9.18–9.48 Nx.

Fig. 3(j) is obtained, with the clear peak corresponding to the cyclic frequency of 50.

If the system properties were not known, it would have been necessary to select the band for the demodulation on the basis of a data-driven index, such as the kurtosis or the RCC. In this case a protrugram based, respectively, on the kurtosis and on the RCC has been calculated, keeping fixed the spectral band amplitude (201 spectral points). The RCC was calculated

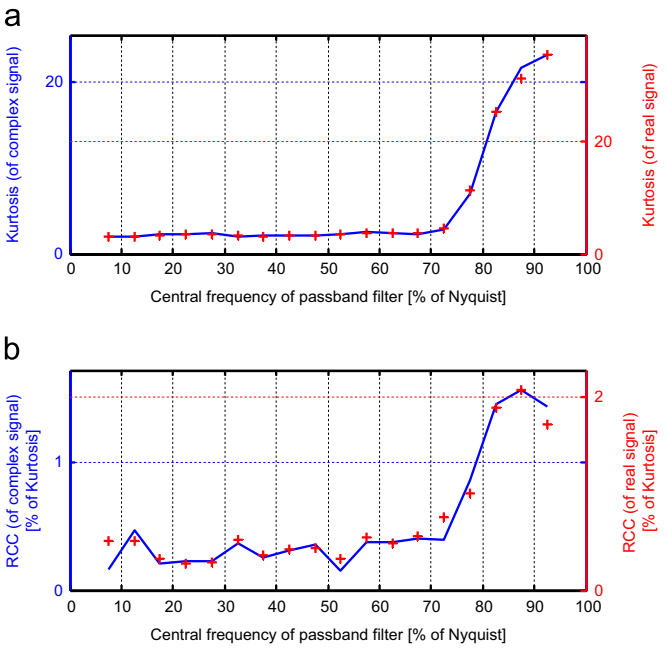


**Fig. 12.** First test – comparison of the FFT-IFFT method vs. time domain filtering method: (a) kurtosis and (b) RCC. (For interpretation of the references to color in this figure caption, the reader is referred to the web version of this paper.)

on the basis of 21 points around the expected cyclic frequency of 50. The results are shown in Fig. 4. It is clear how the RCC (b) shows clearly the best central frequency for the demodulation band, while the kurtosis does not give any clear indication, and rather presents a minimum in correspondence of the optimal frequency. This can be explained by the fact that the impulse response strongly resembles a sinusoidal function, with a lower kurtosis value than noise.

## 5. Experimental endurance tests of rolling element bearings

In order to further prove the validity of the analytical study presented in the previous sections, the results of an extensive experimental activity on rolling element bearings are presented in this section.

### *5.1. First test*

The test-rig of this experimental activity [26] is presented in Fig. 5. Its main subsystem is represented by a traction system taken from a high speed train, and consisting of a 265 kW asynchronous motor (a) and its 26:85 gearbox (b). The output shaft of the gearbox, corresponding to the axle of the bogie in the real application, is here connected to an additional 71:27 gearbox (c), in turn joint to a second asynchronous motor acting as a brake (d). The main subsystem is equipped with a rich set of IEPE accelerometers (100 mV/g sensitivity and 0–10,000 Hz frequency range), in proximity of each bearing, and a tachometer installed on the dummy axle.

A series of test campaigns have been performed on this test rig: on each campaign a different damaged bearing was installed in one of the seven positions available:

1. Motor back: ball bearing.
2. Motor front: cylindrical roller beating.
3. Gearbox input shaft, driven end: cylindrical roller bearing.
4. Gearbox input shaft, non-driven end: cylindrical roller bearing.
5. Gearbox input shaft, non-driven end: ball bearing.
6. Gearbox output shaft (dummy axle), left: tapered roller bearing.
7. Gearbox output shaft (dummy axle), right: tapered roller bearing.

For each campaign, a series of tests in different operating conditions (speed/torque) were performed and vibration data measured and stored. A first example is taken in the case of inner ring damaged bearing installed in position 5 (ball bearing at the non-driven end of the input shaft of the gearbox). The damage, shown in Fig. 6, was produced by electro-discharge machining with a maximum size of approximately 3.6 mm.

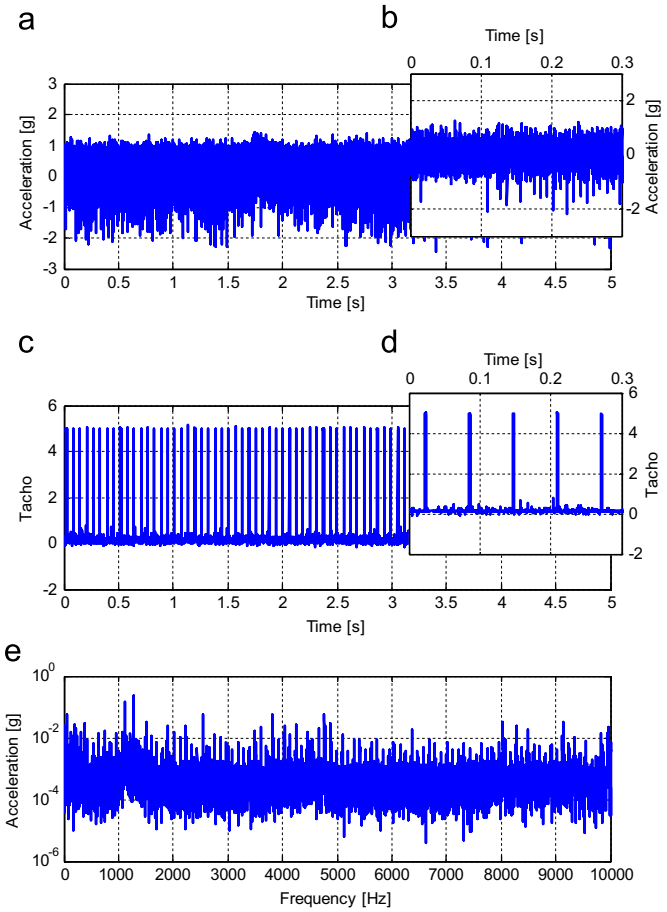


**Fig. 13.** Second test – (a) raw accelerometer signal, (b) zoom of the raw accelerometer signal, (c) raw tachometer signal, (d) zoom of the raw tachometer signal, and (e) spectrum of the raw accelerometer signal.

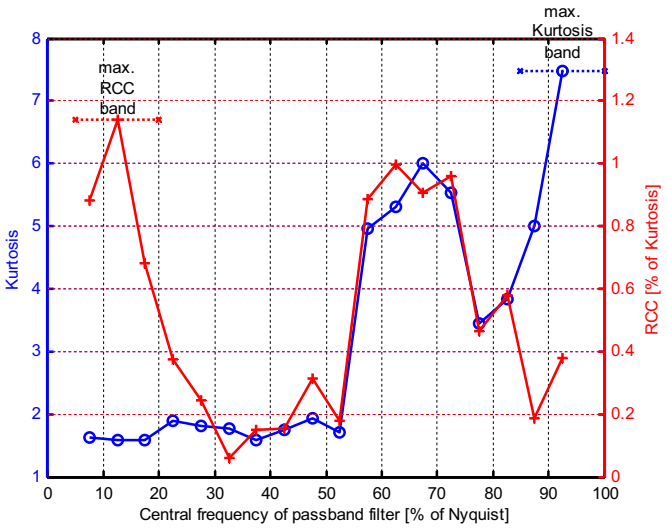


**Fig. 14.** Second test – band selection for the calculation of the SES: comparison among kurtosis and RCC method (Butterworth 4th order filters have been applied to the raw signal for the spectral and cyclic filtering operations).

The test here shown is performed at a constant speed of 16.17 Hz at the dummy axle (52.85 Hz at the gearbox input shaft/motor shaft). The raw vibration signal (a and b) and 1X rev. tachometer signal (c and d) are reported in Fig. 7, together with the spectrum of the raw vibration signal (e).

The vibration data were transformed to the angular domain by means of computed order tracking [27], and then envelope analysis was applied. In this case, given the almost constant speed of the test, the classical envelope procedure was preferred to that proposed in [17], which is more complex and significantly more performing only in case of large speed variations. The resampling was made choosing 1237 samples per revolution, the closest number to the actual average sample rate (20 kHz of sample frequency and 16.17 Hz of 1X rev. speed), in order to reduce to the minimum the distortion introduced in the signal.

The bands were defined for the analysis of the signal with a constant bandwidth 0.15 times the Nyquist frequency, and with an overlap between two subsequent bands of 2/3 the bandwidth.

The kurtosis and RCC for each band were calculated by means of a series of ideal filters in spectral domain and a single ideal filter in the cyclic domain. The results are shown in Fig. 8, respectively, in blue circles-line for the kurtosis and red crosses-line for the RCC. The spectrum in the bands identified by the highest kurtosis and RCC is shown in Fig. 9, in comparison with the one obtained on a healthy bearing. Despite the absence of clear damage specific symptoms, the rise of

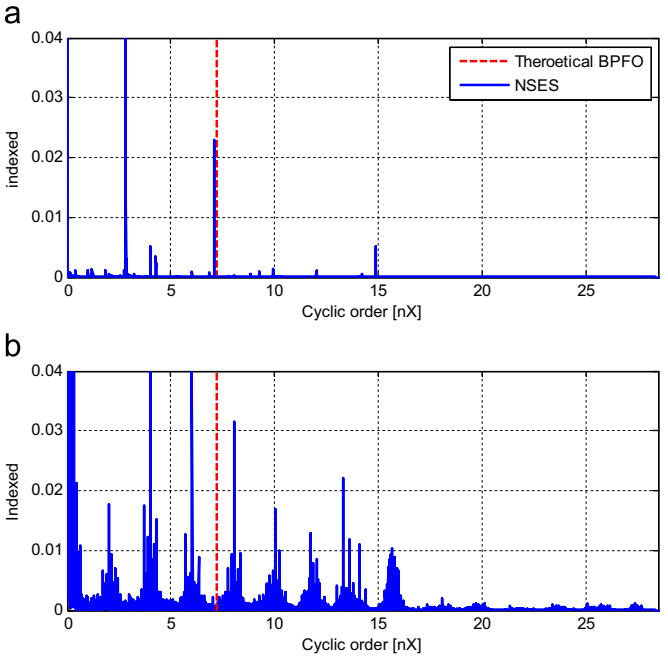


**Fig. 15.** Second test – normalized SESs of (a) optimal RCC band and (b) optimal kurtosis band.

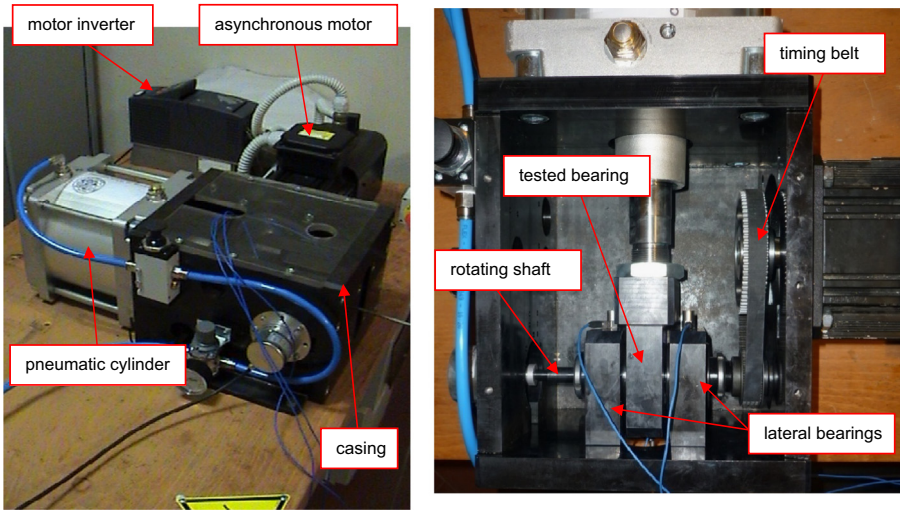


**Fig. 16.** Test-rig for the endurance tests on rolling element bearing – Politecnico di Milano.

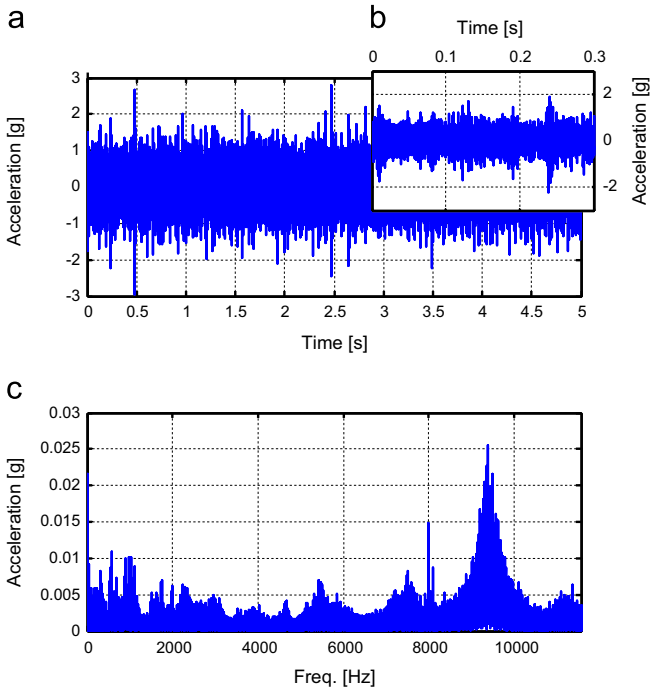


**Fig. 17.** Third test: (a) raw signal, (b) 5-revolutions zoom of the raw signal, and (c) spectrum of the raw signal.

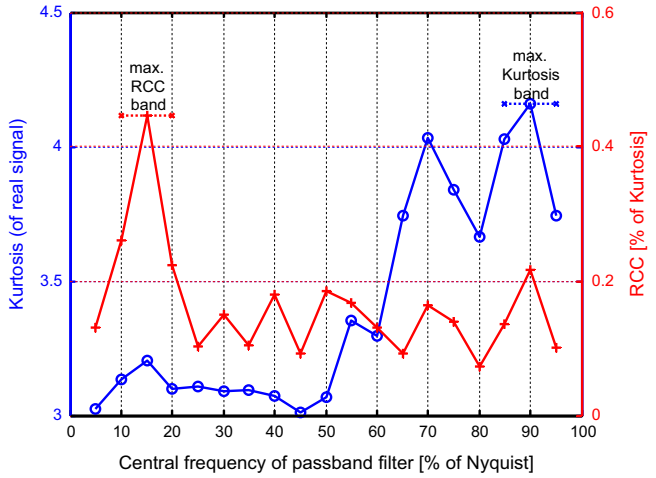


**Fig. 18.** Third test – band selection for the calculation of the SES: comparison among kurtosis and RCC method (Butterwoth 4th order filters have been applied to the raw signal for the spectral and cyclic filtering operations).

the overall energy level and, more significantly, the presence of a recurrent peak (or hill) pattern in the case of damaged bearing suggest that the band carries important diagnostic information.

This is confirmed in Fig. 10(a), which shows the NSES, i.e. standard SES divided by the SES at zero cyclic frequency (Eq. (14)), for both the maximum RCC band (in red line) and the maximum kurtosis band (blue line). The typical peak pattern around the theoretical BPFI clearly identifies the type of damage [17] in both NSESs, however, RCC is characterized by a slight improvement in the amplitude of BPFI peak, sidebands and multiples, with respect to the max kurtosis band. In diagram (b) the cumulate sum of the normalized SESs of diagram (a) is shown moving along the order axis (blue and red lines, respectively, for maximum kurtosis and maximum RCC bands). As demonstrated analytically, the total sum of the peaks of the two normalized SESs converges to the kurtosis (dashed lines) of the corresponding filtered analytic signal.

The correlation of the kurtosis vs. the amplitude of the envelope peaks is also shown in Fig. 11. The evolution of the envelope as a function of the central frequency of the band is tracked in diagram (a), obtained by calculating the normalized SES on a constant bandwidth of 15% the Nyquist frequency, sliding with a step of 5% the Nyquist frequency. It is evident how the symptoms of the damage (peaks around the theoretical BPFI) arise only when the selected band-pass filter is very close

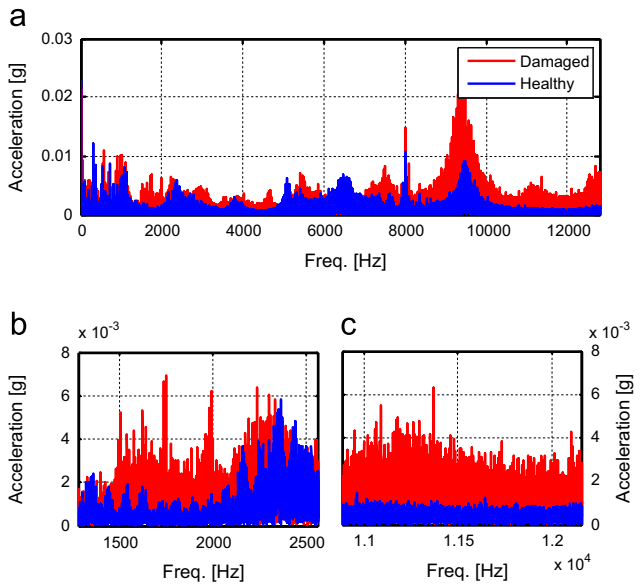


**Fig. 19.** Third test – comparison worn (inner ring damaged) vs. new bearing: (a) full spectrum, (b) zoom in the optimal spectral band indicated by RCC, and (c) zoom in the optimal spectral band indicated by kurtosis.

to the Nyquist frequency. The correlation of this qualitative information with the kurtosis of diagram (b) is a further proof of the equivalence of the two indicators. Moreover, the RCC index is reported in diagram (c), in this case giving similar information to the standard kurtosis.

In Figs. 8, 10 and 11 all the indexes were obtained by means of ideal filters, thus, using FFTs and IFFTs. This, as anticipated above, may be computationally very expensive for the evaluation of a detailed protrugram and can be substituted by the procedure shown in Fig. 2.

To show the effectiveness of the procedure, a series of digital IIR 4th order Butterworth filters has been designed for the spectral bands described before and an additional digital IIR 4th order Butterworth filter has been obtained for the cyclic filtering of the squared signal in the cyclic range 9.18–9.48 Nx of the gearbox input shaft (30–31 Nx of the wheel axle), just about the expected bearing cyclic order of 9.36 Nx of the gearbox input shaft (30.61 Nx of the wheel axle). The raw (fully real) signal has been used instead of the analytic signal, to avoid any transform from and to frequency domain. The results of such estimation are shown in Fig. 12, for the kurtosis (a) and for the RCC (b), obtained by ideal filtering both in spectral and cyclic domain and using the analytic signal (blue lines) and by butterworth spectral and cyclic filters on the raw signal (red crosses). It is clear from diagram (a) that, disregarding a scaling factor of 1.5, due to the application to complex vs. real signals, the kurtosis of each band is very accurately estimated by the filter-bank method. The RCC trend is also correctly estimated (b), with a similar average ratio between the results of the two methods.

In this case, the results of the application of a standard kurtogram or protrugram would have been very similar, owing to the fact that the two indexes indicated as optimal two very close bands, as shown in Fig. 10.

### 5.2. *Second test*

A second example, regarding vibration measurement taken on the electric motor of the same test rig, will show the increased effectiveness of an RCC-based band selection.

In this case, a naturally developed damage was present on the outer ring of the cylindrical roller bearing installed at the motor driving end (DE). In this case the signal is much more disturbed, as clearly visible in Fig. 13(a) and (b), even if in the same conditions of the previous test: the speed is constant at 16.17 Hz of the dummy axle, as it is visible from diagram (c) and (d). The increased noise is probably due to strong electromagnetic fields in proximity of the motor windings.

In order to show the effectiveness of the proposed procedure, the fast version of the algorithm for the calculation of kurtosis and RCC has been directly applied, i.e. applying digital Butterworth filters for both the spectral and the cyclic band-passing and using the raw (real) signal instead of the analytical version. In this case an outer ring damage was expected, with a BPFO at the cyclic frequency of 7.21 Nx of the motor shaft (23.56 Nx of the dummy axle), therefore, the cyclic filter was set to band-pass in the cyclic range 7.04–7.22 Nx of the motor shaft (23–23.6 Nx of the dummy axle). The choice of a band not centered on the theoretical frequency of the damage is due to the fact that deviations of the actual characteristic frequencies of cylindrical roller bearing from the theoretical ones are generally one sided and, for BPFO always negative [17].

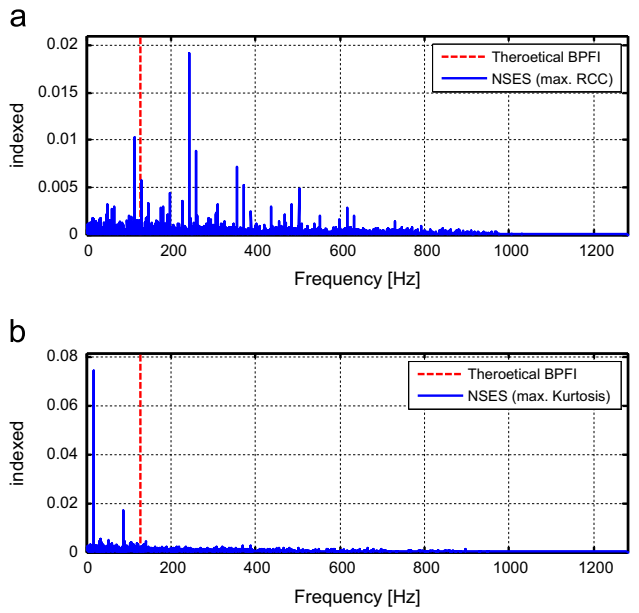


**Fig. 20.** Third test – normalized SESs of (a) optimal RCC band and (b) optimal kurtosis band.

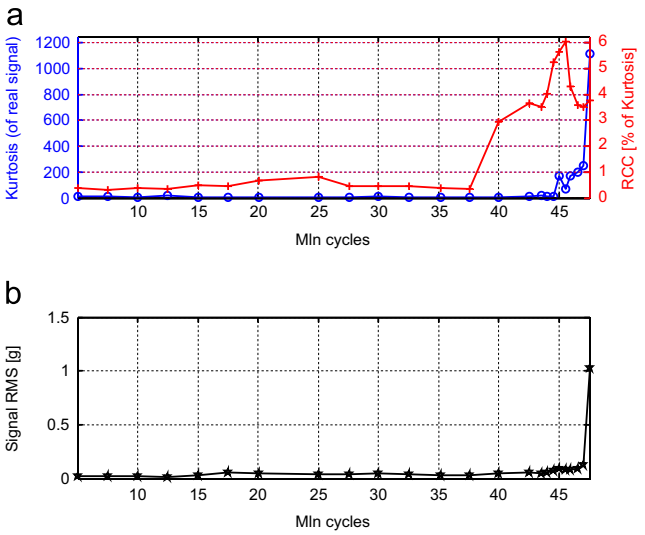


**Fig. 21.** Endurance test – evolution of: (a) kurtosis (blue) and RCC (red), (b) RMS. (For interpretation of the references to color in this figure caption, the reader is referred to the web version of this paper.)

The results are displayed in Fig. 14, where it is clear that the two methods suggest the selection of far different spectral bands for the demodulation of the signal. The very high value of the maximum kurtosis already shows a possible malfunctioning of this criterion.

The SESs calculated on the two different bands are shown in Fig. 15, respectively, for the optimal RCC band (a) and the optimal kurtosis band (b). The improved effectiveness of the RCC is evident.

### *5.3. Third test*

The technique has been also applied to a much smaller test rig to test its validity on bearings with totally different size. This test-rig, shown in Fig. 16, is driven by a 1.75 kW asynchronous motor. The rotating shaft, connected to the motor pulley by a timing belt, is supported by two bearings with double row cylindrical rolling elements lodged in two housing fixed on the external structure. The bearing under test a single row cylindrical roller bearing, model SKF NJ 206 ECP, installed in the middle of the rotating shaft. The casing in which this bearing is installed is connected to a pneumatic cylinder, providing the static load needed to induce internal stresses in the bearing. Vibrations are measured in the radial direction in

correspondence of the bearing by means of a single-axis IEPE accelerometer, with 100 mV/g sensitivity and 0–10,000 Hz frequency range. Signal records are saved at regular intervals of 100,000 cycles with a sample frequency of 25.6 kHz. The speed of the shaft is set to 1000 rpm and the load on the bearing is set to 7500 N.

The analyses have been made on the 5 s signal record of Fig. 17. In this case no order tracking technique has been applied and all the analyses were performed in the actual time/frequency domains.

The results of the application of the 4th order Butterworth filters to the raw signal for the calculation of kurtosis and RCC are shown in Fig. 18. The spectral pass-bands have been defined as before, with a width of 15% of the Nyquist frequency and with an overlap of 2/3 of the bandwidth. For the calculation of the RCC a very narrow band has been chosen from 129 to 131 Hz, expecting a BPFI of 129 Hz and very low upwards deviations of the actual damage frequency (load is high).

The diagrams of Fig. 18 show again significantly different indications for the choice of the bands. Looking at the two bands in Fig. 19(b) and (c) it is difficult to have an assessment of the effectiveness of the two indicators, but it seems that some pattern is present in the RCC optimal band, while a simple increase in the overall spectrum is present for the kurtosis optimal band. The result is clear in the very different quality of the corresponding normalized SESs. In Fig. 20(a), obtained by demodulation of the optimal RCC band, symptoms of inner ring damage are clearly identifiable, while in diagram (b), obtained by demodulating the optimal kurtosis band, no BPFI harmonics is detected.

### 5.4. Prognostic campaign

This tool has also been applied on the same test rig of the third test, with the same bearing and in the same conditions, tracking the evolution in time of the parameters. The evolution of the two indexes, maximum band kurtosis and maximum RCC, is shown in Fig. 21(a), and can be compared with the evolution of the RMS of the signal. It is clear that the bearing failure, which happened after approximately 47 mln cycles is detected first by the RCC, approximately after 40 mln cycles, and only later by the kurtosis, which sees a significant increase only after 45 mln cycles.

## 6. Conclusions

This paper allowed the explicit expression of the strong relationship among squared envelope spectrum, kurtosis and cepstrum pre-whitening. This result could provide a theoretical starting point for the derivation of new indexes and tools for the diagnostic of rolling element bearings and other 2nd order (pseudo-) cyclostationary signals. In particular, in this study it has been used for the selection of a new index, the RCC, able to identify the optimal band for the calculation of the SES itself. The RCC has proven not only more robust than the kurtosis for the selection of the optimal spectral band for demodulation, but also a well performing prognostic tool, able to identify in advance the development of a damage. The narrow cyclic focus of the proposed index may as well entirely substitute the traditional SES, providing as well a much simpler and fast index for an online automatic diagnostic/prognostic of rolling element bearings.

## Appendix A

The proof of the equivalence of the zero-frequency SES value and the fourth power of the RMS is given in this appendix. The starting point is the definition of the SES for a time domain signal $x[n]$, uniformly sampled

$$\mathrm{SES}[k] = |\mathrm{DFT}\{|x[n]|^2\}|^2 = |\mathrm{DFT}\{x[n]\cdot x^*[n]\}|^2 \tag{25}$$

It is then possible to apply the convolution theorem, combined with the properties of the Fourier transform of a complex conjugate quantity:

$$\mathrm{SES}[k] = |X[k] \otimes X^*[-k]|^2 = \left|\sum_h X[h]X^*[h-k]\right|^2 \tag{26}$$

If the SES is then evaluated at zero frequency, the terms in the summation become simple squared magnitudes of the spectrum

$$\mathrm{SES}[0] = \left|\sum_h X[h]X^*[h]\right|^2 = \left|\sum_h |X[h]|^2\right|^2 \tag{27}$$

Their sum represents the squared RMS, finally proving the identity:

$$\mathrm{SES}[0] = |\mathrm{RMS}_x^2|^2 = \mathrm{RMS}_x^4 \tag{28}$$

## References


[1] X. Liu, R.B. Randall, J. Antoni, Blind separation of internal combustion engine vibration signals by a deflation method, Mech. Syst. Signal Process. 22 (5) (2008) 1082–1091. (July).

[2] P.D. McFadden, J.D. Smith, Model for the vibration produced by a single point defect in a rolling element bearing, J. Sound Vib. 96 (1) (1984) 69–82 (8 September).

[3] P. Borghesani, P. Pennacchi, S. Chatterton, R. Ricci, The velocity synchronous discrete Fourier transform for order tracking in the field of rotating machinery (April), Mech. Syst. Signal Process. 18 (2013). (Available online).
[4] P. Pennacchi, A. Vania, S. Chatterton, E. Tanzi, Detection of unsteady flow in a Kaplan hydraulic turbine using machine mechanical model and rotor measured vibrations, in: Proceedings of the ASME Turbo Expo 2012 – GT2012, Paper GT2012-69995, Copenhagen, Denmark, June 11–15, 2012, pp. 1–8.
[5] P. Pennacchi, P. Borghesani, S. Chatterton, A. Vania, Hydraulic instability onset detection in Kaplan turbines by monitoring shaft vibrations, in: Proceedings of the ASME 2012 – International Design Engineering Technical Conferences & Computers and Information in Engineering Conference IDETC/CIE, Paper DETC2012-70963, Chicago, IL, USA, August 12–15, 2012, pp. 1–8.
[6] N. Bachschmid, P. Pennacchi, A. Vania, Steam whirl analysis in a high pressure cylinder of a turbo generator, Mech. Syst. Signal Process.0888-327022 (1) (2008) 121–132.
[7] P. Pennacchi, A. Vania, S. Chatterton, E. Pesatori, Case history of pad fluttering in a tilting-pad journal bearing, in: Proceedings of the ASME Turbo Expo 2010, Power for Land, Sea and Air GT2010, Paper GT2010-22946, Glasgow, UK, ISBN: 978-0-7918-3872-3, June 14–18, 2010, pp. 1–7.
[8] P. Pennacchi, N. Bachschmid, E. Tanzi, Light and short arc rubs in rotating machines: experimental tests and modelling, Mech. Syst. Signal Process.0888-327023 (7) (2009) 2205–2227.
[10] D. Dyer, R.M. Stewart, Detection of rolling element bearing damage by statistical vibration analysis, in: ASME Paper, 26–30 September, 1977.
[11] R.F. Dwyer, Detection of non-Gaussian signals by frequency domain kurtosis estimation, in: International Conference on Acoustics, Speech, and Signal Processing, Boston, 1983, pp. 607–610.
[12] J. Antoni, R.B. Randall, The spectral kurtosis: application to the vibratory surveillance and diagnostics of rotating machines, Mech. Syst. Signal Process. 20 (February (92)) (2006) 308–331.
[13] J. Antoni, Fast computation of the kurtogram for the detection of transient faults, Mech. Syst. Signal Process.0888-327021 (January (1)) (2007) 108–124, http://dx.doi.org/10.1016/j.ymssp.2005.12.002.
[14] T. Barszcz, A. JabŁoński, A novel method for the optimal band selection for vibration signal demodulation and comparison with the kurtogram, Mech. Syst. Signal Process.0888-327025 (January (1)) (2011) 431–451.
[15] J. Antoni, Cyclic spectral analysis of rolling-element bearing signals: facts and fictions, J. Sound Vib. 304 (July (3–5)) (2007) 497–529.
[16] P. Borghesani, P. Pennacchi, R. Ricci, S. Chatterton, Testing second order cyclostationarity in the squared envelope spectrum of non-white vibration signals, Mech. Syst. Signal Process. Available online 15 June 2013, http://dx.doi.org/10.1016/j.ymssp.2013.05.012.
[17] P. Borghesani, R. Ricci, S. Chatterton, P. Pennacchi, A new procedure for using envelope analysis for rolling element bearing diagnostics in variable operating conditions, Mech. Syst. Signal Process. 38 (July (1)) (2013) 23–35.
[18] Y. Zhang, R.B. Randall, Rolling element bearing fault diagnosis based on the combination of genetic algorithms and fast kurtogram, Mech. Syst. Signal Process. 23 (July (5)) (2009) 1509–1517.
[19] N. Sawalhi, R.B. Randall, Spectral kurtosis optimization for rolling element bearings, in: Proceedings of the Eighth International Symposium on Signal Processing and Its Applications, 2005, vol. 2, August 28–31, 2005, p. 839, 842.
[20] E. Bechhoefer, P. Menon, M. Kingsley, Bearing envelope analysis window selection Using spectral kurtosis techniques, in: IEEE Conference on Prognostics and Health Management (PHM), 2011, June 20–23, 2011, p. 1, 6.
[21] W. Kaplan, Advanced Calculus, 4th ed. Addison-Wesley, Reading, MA, 1992, 501.
[22] N. Sawalhi, R. Randall, Signal pre-whitening using cepstrum editing (liftering) to enhance fault detection in rolling element bearings, in: Proceedings of the Twenty-fourth International Congress on Condition Monitoring and Diagnostics Engineering Management (COMADEM), 2011.
[23] N. Sawalhi, R.B. Randall, D. Forrester, Separation and enhancement of gear and bearing signals for the diagnosis of wind turbine transmission systems, Wind Energy (2013), Published online in Wiley Online Library (wileyonlinelibrary.com), doi:10.1002/we.1671.
[24] P. Borghesani, P. Pennacchi, R.B. Randall, N. Sawalhi, R. Ricci, Application of cepstrum pre-whitening for the diagnosis of bearing faults under variable speed conditions, Mech. Syst. Signal Process. 36 (April (2)) (2013) 370–384.
[25] R.B. Randall, J. Antoni, S. Chobsaard, The relationship between spectral correlation and envelope analysis in the diagnostics of bearing faults and other cyclostationary machine signals, Mech. Syst. Signal Process. 15 (September (5)) (2001) 945–962.
[26] P. Borghesani, R. Ricci, S. Chatterton, P. Pennacchi, Fault symptoms of rolling element bearings under variable operating conditions – a multi domain analysis, in: Proceedings of the ASME 2012 – International Design Engineering Technical Conferences & Computers and Information in Engineering Conference IDETC/CIE, Paper DETC2012-70948, Chicago, IL, USA, August 12–15, 2012, pp. 1–7.
[27] K.R. Fyfe, E.D.S. Munck, Analysis of computed order tracking, Mech. Syst. Signal Process. 11 (March (2)) (1997) 187–205.